PAPER

Check for updates

On the relations between the bandgap, structure and composition of the M–Si–N (M = alkali, alkaline earth or rare-earth metal) nitridosilicates†

Otmar M. ten Kate, [ID] ✲[a] Zhijun Zhang[b] and H. T. (Bert) Hintzen[c]

Relations between the bandgap and structural properties and composition of the M–Si–N nitridosilicates (M = alkali, alkaline earth or rare earth metal) have been obtained, using experimental data collected from literature; and qualitative models are presented to explain the observed trends. Compounds with a higher degree of condensation, *i.e.* a higher Si/N ratio, generally have longer M–N bonds and shorter Si–N bonds. The observations can be explained based on the effective charge of N, dependent on its coordination with Si (NSi_x). With increasing Si/N ratio the coordination number of N by Si increases, making the effective charge of the nitrogen atom less negative, resulting in a longer and less covalent M–N bond. This also shifts the N 2p levels down in energy, lowering the top of the valence band (mainly composed of N orbitals); while decreasing the Si–N distance shifts the bottom of the conduction band (mainly composed of Si and M orbitals) upward. Some nitridosilicates show deviations to the general trends, such as γ-Si_3N_4 and several Li-containing compounds. These deviations have been discussed and possible explanations have been given based on peculiarities in their structural characteristics.

1. Introduction

Nitridosilicates have gained a lot of attention over the last years, especially in luminescence research, owing to their large structural diversity and chemical and optical properties.[1,2] When doped with lanthanide ions such as Eu^{2+} or Ce^{3+}, these compounds can show strong emission bands upon excitation with UV or blue light, with emission ranging from the blue to the red region.[1,3] Some of these phosphors have shown high luminescence efficiency in combination with a good thermal and chemical stability, making them highly attractive for luminescence applications. Especially the Eu^{2+} doped nitridosilicates such as $Sr_2Si_5N_8$:Eu^{2+} have shown to be very promising and have been applied as conversion phosphors for phosphor-converted white LEDs (pc-wLEDs).[4–7] Here, a UV or blue LED chip is combined with red- and green-emitting phosphors,

and in the case of a UV LED also blue-emitting phosphors, in order to produce white light with a high colour rendering index. Besides the use in white LEDs, nitridosilicate phosphors are also considered for other applications: as spectral conversion phosphors to enhance solar cell efficiency,[8] as afterglow phosphors,[9] and for LCD backlighting.[10] In addition, the nitridosilicates have also attracted great interest outside the field of luminescence, mainly as ceramic materials[11] due to their chemical resistance, excellent mechanical properties at high temperature and low thermal expansion. It is noteworthy to mention that the nitridosilicates can be modified by replacing some of the Si by Al and N by O, forming silicon aluminium oxy-nitridosilicates, or sialons,[12,13] greatly enhancing the structural diversity. Examples of oxygen and/or aluminium containing nitridosilicate phosphors promising for white LED applications are Eu^{2+} doped Ca-α-sialon,[14,15] $CaAlSiN_3$,[16] β-sialon,[17] and $SrSi_2O_2N_2$.[18,19]

The nitridosilicates are compounds with the overall composition of $M_xSi_yN_z$ where M is an alkali (1+), alkaline earth (2+) or rare-earth (3+) metal ion or combination thereof. The structures generally consist of a framework of interconnected SiN_4 tetrahedra with the metal ions located in the cavities of the framework. This makes the nitridosilicates comparable to the oxosilicates, which consist of interconnected SiO_4 tetrahedra. However, in the oxosilicates the O atoms are usually one-fold or twofold coordinated by Si, with only a few compounds showing

[a] *Product and Process Engineering, Chemical Engineering, Applied Sciences, Delft University of Technology, Van der Maasweg 9, 2629 HZ, Delft, The Netherlands. E-mail: o.m.tenkate@tudelft.nl*

[b] *School of Materials Science and Technology, Shanghai University, Shanghai, 200444, China*

[c] *Luminescent Materials Group, Radiation Science and Technology, Applied Sciences, Delft University of Technology, Mekelweg 15, 2629 JB, Delft, The Netherlands*

threefold coordination, as occurs in high-pressure phase stishovite (SiO_2).[20] In the nitridosilicates on the other hand, in addition to terminal (NSi_1) and bridging (NSi_2) nitrogen, the threefold coordination of N by Si (NSi_3) is much more common, and N can even be fourfold coordinated by Si (NSi_4). This allows for a much wider range of structures ranging from highly condensed Si_3N_4 with low M/Si ratio and high degree of condensation (Si/N ratio is 0.75), to Ca_4SiN_4 with a very low degree of condensation (Si/N ratio is 0.25) as a consequence of a high M/Si ratio. Such structural features strongly determine the chemical stability of the materials, showing a lower stability for compounds with a lower degree of cross-linking between SiN_4 tetrahedra.[21] Nitridosilicates such as Ca_4SiN_4[22,23] and Eu_2SiN_3[24] with a low degree of cross-linking are highly sensitive to water, while $BaSi_7N_{10}$[25] with a high degree of cross-linking is very stable against oxidation and not corroded by water.

In addition to stability variations among the nitridosilicate structures, there is also a large variation in their optical properties depending on the chemical composition (*i.e.* M/Si ratio). The bandgap of the $M_xSi_yN_z$ compounds can vary greatly from as small as 2.7 eV in Li_8SiN_4[26] to as large as 6.9 eV in $LiSi_2N_3$.[27,28] This has its influence on the performance as a luminescent material when the nitridosilicate host lattice is doped with lanthanide ions. For example, the position of the lowest 5d level of Eu^{2+} with respect to the bottom of the conduction band strongly influences the efficiency and thermal stability of the Eu^{2+} 5d–4f emission. When positioned inside or close to the conduction band, auto-ionization or thermal ionization of the 5d electron to the conduction band may occur and the 5d–4f emission will be quenched.[29] Other examples are the position of the valence band with respect to the lanthanide 4f ground states that determines the energy of charge transfer transitions,[30] and the position of the 4f ground state of the divalent ion with respect to the valence and conduction band that determines the valence stability of a divalent ion.[31] These examples demonstrate the importance for the development of luminescent materials to know how the positions of the valence and conduction band of the phosphor host lattice are influenced by its composition and can be tuned.

This work presents the relations between the composition, structural properties and bandgap of the nitridosilicates and presents qualitative models that can explain the observed trends. For this we collect and analyse experimental data presented in literature on all $M_xSi_yN_z$ nitridosilicates where M is an alkali (1+), alkaline earth (2+) or rare earth (3+) metal or combination thereof. In the first part of the manuscript we discuss the structural characteristics of the nitridosilicates, such as bond lengths and coordination numbers, and relate it to the chemical compositions of the materials. A qualitative model is then developed to explain the influence that the Si/N ratio has on the bond lengths and coordination numbers. In the final part of the manuscript the relation between the bandgap and the structure and composition of the nitridosilicates is discussed. A second model is then developed to explain the influence of the Si/N ratio on the positions of the valence and conduction band.

2. The influence of chemical composition on crystal structure, bond lengths and bandgap

The nitridosilicates considered in this work (see Table 1) are all compounds with the general composition $M_xSi_yN_z$ where M is a monovalent alkali (A = Li^+), divalent alkaline earth (AE = Mg^{2+}, Ca^{2+}, Sr^{2+}, Ba^{2+}), or trivalent rare-earth (RE = Sc^{3+}, Y^{3+}, La^{3+}, or other trivalent lanthanide) metal ion, or combination thereof. M may also be a divalent rare earth (*e.g.* Eu^{2+}). Also included in this work is $Ca_{0.8}Y_{1.2}Si_4N_{6.8}C_{0.2}$,[32] because it only contains a small amount of carbon and is closely related to the other nitridosilicates. The structure is very similar to the pure nitride $(AE)(RE)Si_4N_7$ (AE = Ca, Sr, Ba; RE = Sc, Y, Lu, Yb) compounds,[33] but is a disordered variant where nitrogen is partly replaced by carbon for charge compensation and a part of the Y^{3+} ions is present on the Ca^{2+} sites.[32] The lithium and magnesium containing nitridosilicates such as Li_5SiN_3, $Li_4Ca_3Si_2N_6$, $Li_4CaMg_2Si_2N_6$, $MgSiN_2$ and $SrMg_3SiN_4$ have also been included, for the sake of comparison, even though it may be argued that some these compounds are not really nitridosilicates but nitrido-lithosilicates or nitrido-magnesosilicates because Li and Mg can be considered part of the nitridosilicate framework. This issue will be further discussed in this manuscript. The structural characteristics of all the nitridosilicates have been collected from experimental data from literature and are summarized in Table 1.

2.1 Crystal structure

Depending on the M/Si ratio of the nitridosilicates, different ways of N by Si coordination exist, as illustrated in Fig. 1. The non-metal silicon nitrides α-Si_3N_4[34,79] and β-Si_3N_4[35,80] both consist of a three-dimensional network of corner-sharing SiN_4 tetrahedra. All N atoms are coordinated by three Si atoms. As a result of its high degree of cross-linking between SiN_4 tetrahedra, Si_3N_4 exhibits an outstanding chemical, thermal and mechanical stability. When introducing metals into the structure, Si–NSi_2 bonds will be broken, reducing the degree of cross-linking between SiN_4 tetrahedra. As a result, compounds such as $(AE)Si_7N_{10}$ (AE = Sr, Ba),[25,49] $(AE)_2Si_5N_8$ (AE = Ca, Sr, Ba),[46,48] $LaSi_3N_5$[56,81] and $La_3Si_6N_{11}$[56] have N atoms both threefold and twofold coordinated by Si. However, the SiN_4 tetrahedra still form a three-dimensional network of corner-sharing or, as is the case for $(AE)Si_7N_{10}$, also edge-sharing tetrahedra. In compounds such as $BaYbSi_4N_7$[82] and $Ca_3Sm_3Si_9N_{17}$[73] there is no threefold coordination, but unusual fourfold coordination of N by Si exists in addition to the twofold coordination. All N atoms are twofold coordinated by Si in α-$CaSiN_2$, $SrSiN_2$ and $BaSiN_2$.[44] In compounds with quite high M/Si ratios resulting in low Si/N ratios, N atoms can also be singly bonded by Si, as occurs partly in Eu_2SiN_3[24] and $La_5Si_3N_9$.[54] In these compounds the SiN_4 tetrahedra form non-branched (in Eu_2SiN_3) or branched (in $La_5Si_3N_9$) linear chains. In $(AE)_5Si_2N_6$ (AE = Ca, Ba)[23,43,51] and Ca_4SiN_4[23] the SiN_4 tetrahedra do not form interconnected networks anymore, but are isolated units (in Ca_4SiN_4) or form isolated Si_2N_6 pairs consisting of two edge-sharing tetrahedra (in $(AE)_5Si_2N_6$).

Table 1 Experimentally determined structural characteristics of the nitridosilicates ($M_xSi_yN_z$) collected from literature

Compound	Space group	ICSD	Si–N network (CS = corner sharing, ES = edge sharing, 3D = 3-dimensional)	N by Si coordination $N^{[x]}$	Average M–N distance (Å)	Shortest Si–N distance[a] (Å)	Ref.
α-Si_3N_4	(159)	79 797	3D CS SiN_4 network	$N^{[3]}$	—	1.673	34
β-Si_3N_4	(173)	8263	3D CS SiN_4 network	$N^{[3]}$	—	1.704	35
γ-Si_3N_4	(227)	97 566	3D ES/CS SiN_4/SiN_6 network	$N^{[4]}$	—	1.853	36
$Li_{21}Si_3N_{11}$	(79)	191 135	[b]	[b]	2.111	1.656	37
Li_5SiN_3	(206)	25 582	[b]	[b]	2.084	1.910	38
Li_2SiN_2	(61)	420 126	3D CS SiN_4 network	$N^{[2]}$	2.160	1.728	39
$LiSi_2N_3$	(36)	98 524	3D CS SiN_4 network	$1N^{[2]}:2N^{[3]}$	2.263	1.681	40
$MgSiN_2$	(33)	90 731	3D CS SiN_4 network	$N^{[2]}$	2.249	1.732	41
$Mg_2Si_5N_8$	(9)		3D CS SiN_4 network	$1N^{[2]}:1N^{[3]}$	2.305	1.660	42
Ca_4SiN_4	(14)	250 872	Isolated SiN_4 tetrahedrons	$N^{[1]}$	2.522	1.767	23
α-$Ca_5Si_2N_6$	(15)	414 462	Isolated pairs of ES SiN_4	$2N^{[1]}:1N^{[2]}$	2.575	1.713	43
β-$Ca_5Si_2N_6$	(12)	250 873	Isolated pairs of ES SiN_4	$2N^{[1]}:1N^{[2]}$	2.578	1.735	23
α-$CaSiN_2$	(61)	170 267	3D CS SiN_4 network	$N^{[2]}$	2.583	1.729	44
$Ca_{16}Si_{17}N_{34}$[c]	(216)	248 945	3D CS SiN_4 network	$2N^{[1]}:14N^{[2]}:1N^{[4]}$	2.536	1.645	45
$Ca_2Si_5N_8$	(9)	79 070	3D CS SiN_4 network	$1N^{[2]}:1N^{[3]}$	2.646	1.671	46
β-$Ca_2Si_5N_8$	(4)		3D CS SiN_4 network	$1N^{[2]}:1N^{[3]}$	2.730	1.618	42
HP-$Ca_2Si_5N_8$	(61)	419 318	3D CS SiN_4 network	$1N^{[2]}:1N^{[3]}$	2.577	1.664	47
$SrSiN_2$	(14)	170 270	3D CS/ES SiN_4 network	$N^{[2]}$	2.859	1.711	44
$Sr_2Si_5N_8$	(31)	401 500	3D CS SiN_4 network	$1N^{[2]}:1N^{[3]}$	2.949	1.675	48
$SrSi_7N_{10}$	(7)	154 166	3D CS and ES SiN_4 network	$1N^{[2]}:4N^{[3]}$	3.069	1.683	49
$SrSi_6N_8$	(44)	319 265	3D CS SiN_4 network (Si–Si bonds)	$1N^{[2]}:3N^{[3]}$	3.028	1.691	50
$Ba_5Si_2N_6$	(19)	81 570	Isolated pairs of ES SiN_4	$2N^{[1]}:1N^{[2]}$	2.862	1.747	51
$BaSiN_2$	(64)	170 268	3D CS/ES SiN_4 network	$N^{[2]}$	2.991	1.719	44
$Ba_2Si_5N_8$	(31)	401 501	3D CS SiN_4 network	$1N^{[2]}:1N^{[3]}$	2.999	1.686	48
$BaSi_7N_{10}$	(7)	405 772	3D CS and ES SiN_4 network	$1N^{[2]}:4N^{[3]}$	3.269	1.683	25
$BaSi_6N_8$	(44)	417 444	3D CS SiN_4 network (Si–Si bonds)	$1N^{[2]}:3N^{[3]}$	3.062	1.667	52
$Eu_2Si_5N_8$	(31)	59 257	3D CS SiN_4 network	$1N^{[2]}:1N^{[3]}$	2.894	1.681	53
$La_5Si_3N_9$	(64)	419 064	Branched chains of CS SiN_4	$2N^{[1]}:1N^{[2]}$	2.711	1.564	54
$La_3Si_6N_{11}$	(100)	248 709	3D CS SiN_4 network	$9N^{[2]}:2N^{[3]}$	2.676	1.711	55
$LaSi_3N_5$	(19)	130 022	3D CS SiN_4 network	$3N^{[2]}:2N^{[3]}$	2.802	1.690	56
$Ce_5Si_3N_9$	(64)	419 063	Branched chains of CS SiN_4	$2N^{[1]}:1N^{[2]}$	2.685	1.725	54
$Ce_7Si_6N_{15}$ (tricl.)	(2)	420 199	3D CS SiN_4 network	$2N^{[1]}:5N^{[2]}$	2.772	1.705	57
$Ce_7Si_6N_{15}$ (trig.)	(148)	420 200	3D CS SiN_4 network	$2N^{[1]}:5N^{[2]}$	2.770	1.625	57
$Ce_3Si_6N_{11}$	(100)	237 444	3D CS SiN_4 network	$9N^{[2]}:2N^{[3]}$	2.661	1.725	58
$CeSi_3N_5$	(19)	402 910	3D CS SiN_4 network	$3N^{[2]}:2N^{[3]}$	2.783	1.686	56
$Pr_5Si_3N_9$	(64)	260 288	Branched chains of CS SiN_4	$2N^{[1]}:1N^{[2]}$	2.672	1.719	59
$Pr_7Si_6N_{15}$	(2)	420 201	3D CS SiN_4 network	$2N^{[1]}:5N^{[2]}$	2.762	1.693	57
$Pr_3Si_6N_{11}$	(100)	402 178	3D CS SiN_4 network	$9N^{[2]}:2N^{[3]}$	2.646	1.703	60
$Sm_3Si_6N_{11}$	(100)	80 183	3D CS SiN_4 network	$9N^{[2]}:2N^{[3]}$	2.618	1.697	56
$Li_4Ca_3Si_2N_6$	(12)	420 675	Isolated pairs of ES SiN_4[d]	$2N^{[1]}:1N^{[2]}$	2.596 (Ca)	1.711	61
$Li_4Sr_3Si_2N_6$	(12)	421 259	Isolated pairs of ES SiN_4[d]	$2N^{[1]}:1N^{[2]}$	2.735 (Sr)	1.735	61
$Li_4Ca_2MgSi_2N_6$	(12)	427 077	Isolated pairs of ES SiN_4[d]	$2N^{[1]}:1N^{[2]}$	2.482 (Ca)	1.743	62
$Li_2Ca_2Mg_2Si_2N_6$	(12)	427 078	Isolated pairs of ES SiN_4[d]	$2N^{[1]}:1N^{[2]}$	2.588 (Ca)	1.720	62
$Li_2Ca_3MgSi_2N_6$	(12)		Isolated pairs of ES SiN_4[d]	$2N^{[1]}:1N^{[2]}$	2.554 (Ca)	1.720	63
$Li_2Sr_4[Si_2N_5]N$	(119)	422 596	Layered CS SiN_4 network	$1N^{[0]}:2N^{[1]}:3N^{[2]}$	2.694 (Sr)	1.751	64
$LiCa_3Si_2N_5$	(15)	420 676	Double chain of ES/CS SiN_4	$2N^{[1]}:1N^{[2]}$	2.540 (Ca)	1.726	65
$Li_2CaSi_2N_4$	(205)	421 548	3D CS SiN_4 network	$N^{[2]}$	2.528 (Ca)	1.714	66
$Li_2SrSi_2N_4$	(205)	421 549	3D CS SiN_4 network	$N^{[2]}$	2.699 (Sr)	1.738	66
$Li_5La_5Si_4N_{12}$	(117)	421 528	Non-br. chains CS SiN_4	$2N^{[1]}:1N^{[2]}$	2.609 (La)	1.740	67
$Li_5Ce_5Si_4N_{12}$	(117)	421 527	Non-br. chains CS SiN_4	$2N^{[1]}:1N^{[2]}$	2.605 (Ce)	1.709	67
$CaMg_3SiN_4$	(88)	427 074	Isolated SiN_4 tetrahedrons[d]	$N^{[1]}$	2.638 (Ca)	1.763	68
$SrMg_3SiN_4$	(88)	427 076	Isolated SiN_4 tetrahedrons[d]	$N^{[1]}$	2.802 (Sr)	1.791	68
$EuMg_3SiN_4$	(88)	427 075	Isolated SiN_4 tetrahedrons[d]	$N^{[1]}$	2.680 (Eu)	1.757	68
$BaMg_3SiN_4$	(2)	428 510	3D CS $(Si,Mg)N_4$ network	—	2.953 (Ba)	1.892	69
$Ba_4MgSi_2N_6$	(70−2)	187 335	Isolated pairs of ES SiN_4	$2N^{[1]}:1N^{[2]}$	2.953 (Ba)	1.739	70
$Ba_3Ca_2Si_2N_6$	(15)	187 336	Isolated pairs of ES SiN_4	$2N^{[1]}:1N^{[2]}$	2.910 (Ba)	1.730	70
$Ba_{1.6}Sr_{3.4}Si_2N_6$	(15)	187 337	Isolated pairs of ES SiN_4	$2N^{[1]}:1N^{[2]}$	[e]	1.718	70
$CaLaSiN_3$	(64)		Non-branched chains CS SiN_4	$2N^{[1]}:1N^{[2]}$			71
Eu_2SiN_3	(64)	420 679	Non-branched chains CS SiN_4	$2N^{[1]}:1N^{[2]}$	2.764 (Eu^{2+})	1.731	24
$Ba_2Nd_7Si_{11}N_{23}$	(65)	407 202	3D CS SiN_4 zeolite network	$2N^{[1]}:21N^{[2]}$	3.164 (Ba)	1.685	72
$Ca_3Sm_3Si_9N_{17}$	(215)	421 644	3D CS SiN_4 network	$16N^{[2]}:1N^{[4]}$	[e]	1.696	73
$Ca_3Yb_3Si_9N_{17}$	(215)	421 645	3D CS SiN_4 network	$16N^{[2]}:1N^{[4]}$	[e]	1.687	73
$Ba_{1.5}Eu_{1.5}YbSi_6N_{11}$	(198)	407 300	3D CS SiN_4 network	$9N^{[2]}:2N^{[3]}$	3.012 (Ba)	1.701	74
$SrScSi_4N_7$	(186)	189 117	3D CS SiN_4 network	$6N^{[2]}:1N^{[4]}$	2.957 (Sr)[f]	1.688[f]	75
$CaYSi_4N_7$[g]	(186)	152 975	3D CS SiN_4 network	$6N^{[2]}:1N^{[4]}$	[e]	1.709	32
$SrYSi_4N_7$	(186)	150 459	3D CS SiN_4 network	$6N^{[2]}:1N^{[4]}$	3.012 (Sr)	1.699	76
$BaYSi_4N_7$	(186)	98 276	3D CS SiN_4 network	$6N^{[2]}:1N^{[4]}$	3.014 (Ba)	1.701	77
$EuYSi_4N_7$	(186)	150 460	3D CS SiN_4 network	$6N^{[2]}:1N^{[4]}$	3.019 (Eu)	1.668	76

11506 | J. Mater. Chem. C, 2017, 5, 11504–11514

This journal is © The Royal Society of Chemistry 2017

Table 1 (continued)

Compound	Space group	ICSD	Si–N network (CS = corner sharing, ES = edge sharing, 3D = 3-dimensional)	N by Si coordination $N^{[x]}$	Average M–N distance (Å)	Shortest Si–N distance^a (Å)	Ref.
SrYbSi$_4$N$_7$	(186)	405 625	3D CS SiN$_4$ network	$6N^{[2]}$:$1N^{[4]}$	2.996 (Sr)	1.708	78
EuYbSi$_4$N$_7$	(186)	592 58	3D CS SiN$_4$ network	$6N^{[2]}$:$1N^{[4]}$	2.993 (Eu)	1.713	53
BaYbSi$_4$N$_7$	(186)	405 194	3D CS SiN$_4$ network	$6N^{[2]}$:$1N^{[4]}$	3.017 (Ba)	1.717	78

^{a} If there are multiple Si sites with different Si–N distances in a structure, the average is taken of the shortest Si–N distance of each site. ^{b} Li$_{21}$Si$_3$N$_{11}$ and Li$_5$SiN$_3$ both crystallize in an anti-fluorite (Li,Si)$_2$N structure with N 8-fold coordinated by Si and Li. ^{c} Ca$_{16}$Si$_{17}$N$_{34}$ is also known as cubic-CaSiN$_2$. ^{d} Structures may also be considered a 3D network of corner-sharing and edge-sharing SiN$_4$ and LiN$_4$ and/or MgN$_4$ tetrahedra. ^{e} Compound contains mixed Sr/Ba, Ca/Sm, Ca/Yb or Ca/Y sites. ^{f} Distances based on a structure doped with 5% Eu. ^{g} CaYSi$_4$N$_7$ is actually Ca$_{0.8}$Y$_{1.2}$Si$_4$N$_{6.8}$C$_{0.2}$.
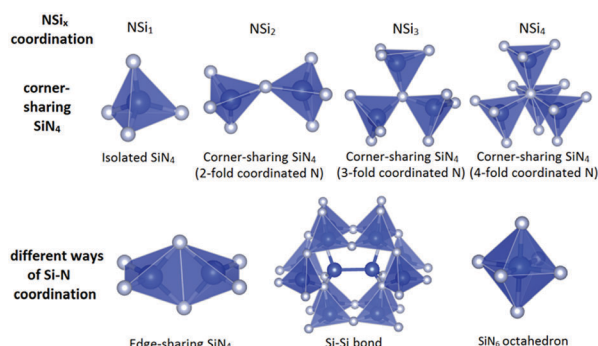
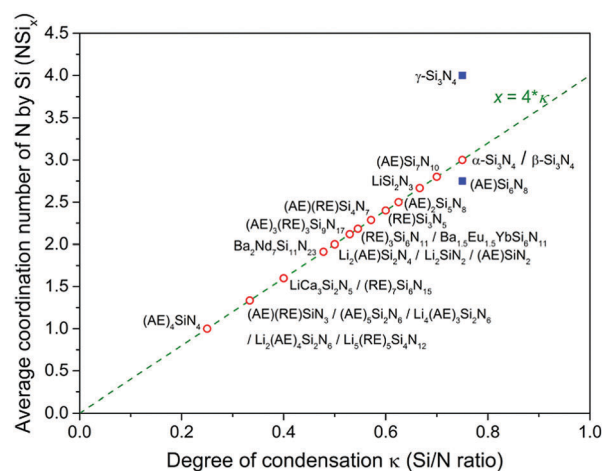Fig. 1 Various ways of Si–N coordination in nitridosilicates.

Fig. 2 Average coordination number x of N by Si (NSi$_x$) versus the degree of condensation κ (Si/N ratio) of the nitridosilicates. The green dashed line indicates the linear relationship $x = 4 \times \kappa$. Compounds that follow this relation are indicated by open red circles, compounds that do not are indicated by solid blue squares.

In all the previously mentioned cases, the Si and N atoms are present in SiN$_4$ tetrahedra. As a consequence, there is a direct relation between the degree of condensation κ (here defined as the Si/N ratio) and the average coordination number x of nitrogen by silicon (NSi$_x$), with $x = 4 \times \kappa$, as is shown in Fig. 2. There are a just few nitridosilicates in which not all Si and N atoms are present in SiN$_4$ tetrahedra and the relation $x = 4 \times \kappa$ is not followed: γ-Si$_3$N$_4$ and (AE)Si$_6$N$_8$ (AE = Sr, Ba), which are indicated with blue squares in Fig. 2. In γ-Si$_3$N$_4$ with cubic spinel structure[83] all N atoms are fourfold coordinated by Si and SiN$_6$ octahedra exist in addition to SiN$_4$ tetrahedra. In (AE)Si$_6$N$_8$ (AE = Sr, Ba)[50,52] N$_3$Si–SiN$_3$ entities are present in which two Si atoms are directly bonded to each other.

The M cations are the positive counterions of the negative nitridosilicate framework and are located in the cavities of the network. They are usually coordinated by six or more N atoms. However, if the metal ion is relatively small, as is the case for Mg^{2+} and Li$^+$, they can also form TN$_4$ (T = Mg, Li) tetrahedrons similar to the SiN$_4$ tetrahedrons. It may then be more appropriate to consider them part of the framework instead of as counterions. This is for example the case in Li$_5$SiN$_3$ with anti-fluorite structure where Si and Li are located on mixed sites forming (Si,Li)N$_4$ tetrahedrons.[37,38] In several other Li and Mg containing nitridosilicates the situation is however less obvious. Li$_4$Ca$_3$Si$_2$N$_6$ consists of SiN$_4$ and LiN$_4$ tetrahedra with octahedrally coordinated Ca^{2+} ions in between, so Si and Li can be considered part of the 3D framework and the compound could be written as Ca$_3$[Li$_4$Si$_2$N$_6$].[61,62] However, for the same structure one of the Ca^{2+} ions can be replaced by two Li$^+$ ions, while at the same time 4 Li$^+$ ions are replaced by 2 Mg^{2+} ions resulting in Li$_2$Ca$_2$[Mg$_2$Si$_2$N$_6$] in which tetrahedrally coordinated

Mg is now part of the framework and Li$^+$ is now a counterion forming [Li$_2$]N$_6$ octahedra.[62] Starting form Ca$_3$[Li$_4$Si$_2$N$_6$] the Mg can also be positioned on a Ca site, while the remaining Ca^{2+} ions switch positions with the Li$^+$ ions on the [Li$_2$]N$_6$ positions, forming Ca$_2$Mg[Li$_4$Si$_2$N$_6$] in which now Li is part of the framework in a tetrahedral coordination and Mg^{2+} is a counterion in a fourfold planar rectangular coordination.[62]

However, because Li$^+$ and Mg^{2+} have a larger ionic radius, a lower electronegativity, and a lower oxidation number than Si^{4+}, the influence of Li$^+$ and Mg^{2+} on parameters like bond lengths and bandgap will be different. Consequently, it is not appropriate to simply add up the Si, Li and Mg atoms and use the (Si + Mg + Li)/N ratio as the principal parameter. Therefore, the Si/N ratio is used as the principal parameter in this manuscript, even when Mg and/or Li may be considered part of the cross-linking framework. As a result, a compound like Ba[Mg$_3$SiN$_4$] that is reported[69] to have a degree of condensation of 1 based on its (Mg + Si)/N ratio, is listed as a compound with a Si/N ratio of 0.25 in this work.

2.2 Bond lengths

Since N is in the −III oxidation state and Si in the +IV oxidation state, the effective charge of the N atom will be zero if it is threefold coordinated by tetrahedrally coordinated Si atoms (NSi$_3$).
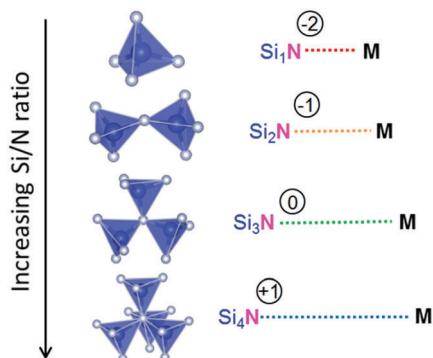
This journal is © The Royal Society of Chemistry 2017

J. Mater. Chem. C, 2017, 5, 11504–11514 | 11507

Fig. 3 Increase of the M–N bond length with increasing N by Si coordination.

In twofold coordination (NSi_2), the N atom is under-bonded, causing it to be effectively -1 negatively charged. This will therefore result in a stronger, more covalent interaction between N and the positively charged metal ion M in the structure. It can therefore be expected that the M–N bond will be shorter when N is in NSi_2 coordination than when N is in the ideal NSi_3 coordination. If the N atom is only terminally coordinated by Si (NSi_1) this effect will become more pronounced. *Vice versa*, a less covalent interaction and longer M–N bond can be expected if the N atom is over-bonded in a fourfold coordination by Si. This means that one may expect an increase of the average M–N distance with increasing Si/N ratio, as schematically illustrated in Fig. 3.

As expected, a larger M–N distance with increasing Si/N ratio is indeed the trend that can be qualitatively observed from the experimental data collected from literature (Table 1), and shown in Fig. 4. For the Ca, Sr, Ba and La sites the average distance to nitrogen tends to increase with increasing Si/N ratio in correspondence with a more positive effective charge for N. It should be noted here that, even though a linear fit through the data is presented, this does not imply that the relation between Si/N ratio and M–N distance should be linear. The purpose of the linear fit is to show that there seems to be a general trend showing an increase of M–N distance with increasing Si/N ratio, but several secondary effects might be present that cause an increased scattering of the data. Nevertheless, the deviation from the general trend is in most compounds less than 0.05 Å. The strongest increase of M–N distance with increasing Si/N ratio is observed for M = Sr, while the increase is weakest for M = Ca. The reason for the surprising order Sr–N > Ba–N > Ca–N (while in terms of size and atomic number Ba > Sr > Ca) is unclear and further studies would be necessary to clarify its cause. It might be a consequence of scattering of the data due to secondary effects as some data points have a relatively strong influence on the steepness of the slope.

For the Ca sites, the increase of the Ca–N distance with increasing Si/N ratio is rather limited with only about 0.1 Å difference between Ca_4SiN_4 and $Ca_2Si_5N_8$. This makes the increase smaller than the scattering of the data. For example, among the compounds with a Si/N ratio of 1/3, $Li_4Ca_3Si_2N_6$ has an almost 0.2 Å larger average Ca–N bond length than $Li_4Ca_2MgSi_2N_6$. As was discussed above $Li_4Ca_2MgSi_2N_6$ is homeotypic to $Li_4Ca_3Si_2N_6$ but Ca^{2+} ions have been partly replaced by Mg^{2+} ions and the

remaining Ca^{2+} ions have switched places with the Li^+ ions, which can explain the relatively short Ca–N bond length in $Li_4Ca_2MgSi_2N_6$. For the Sr sites the absolute scattering of the data is similar as for the Ca sites. However, among the Sr sites there is a large increase of the Sr–N distance with increasing degree of condensation, making the scattering relatively small. For the Ba sites the observed dependence on Si/N ratio is also strong, but the deviation from the general trend is quite large for $BaSi_7N_{10}$ and $Ba_2Nd_7Si_{11}N_{23}$, having relatively large Ba–N distances. This may be due to the large coordination numbers for Ba in these compounds. In $BaSi_7N_{10}$ the coordination number is 13,[25] while in Ba_2Nd_7-$Si_{11}N_{23}$, which has an unusual zeolite-analogous structure,[72] the coordination number of some of the Ba atoms goes up to even 16.

Some scattering in the data of Fig. 4 may also be due to the fact that the Si/N ratio, which basically is a measure for the average N coordination number (see Fig. 2), may not exactly represent the actual N by Si coordination number of the N atoms surrounding the metal ion. In $BaYSi_4N_7$ for example, the N atoms have an average coordination number of 2.29 because the ratio of twofold/fourfold coordinated N atoms is 6/1. However, the N atoms surrounding Ba have an average coordination number of 2 as the fourfold coordinated N atoms are far away from and not coordinated to Ba. In addition, the scattering of the data in Fig. 4 may be enhanced due to the presence of different types of metal ions M within one compound.

While the M–N bond lengths increase with increasing degree of condensation, the Si–N bond lengths tend to decrease with increasing degree of condensation, as has previously been observed by Schnick *et al.*[12,84] This can also be observed from the data shown in Fig. 5a: the average Si–N distance is relatively large in for example Ca_4SiN_4 (1.791 Å) with very low degree of condensation, while relatively small in $SrSi_7N_{10}$ (1.731 Å) with a very high degree of condensation.

If the shortest Si–N distance is plotted *versus* the Si/N ratio (Fig. 5b) instead of the average Si–N distance (Fig. 5a), a similar trend is observed. The correlation of the data is then somewhat stronger, considering that the Pearson correlation coefficient changes from -0.53 for the fit of the average Si–N distance *versus* Si/N ratio to -0.67 for fit of the shortest Si–N distance *versus* Si/N ratio. Note that the slope of the trend line in Fig. 5b (shortest Si–N distance) is also steeper than in Fig. 5a (average Si–N distance).

A few compounds do not follow the general trend in Fig. 5a and b and have either a relatively large or relatively small shortest Si–N bond. Among them is γ-Si_3N_4 with a relatively large Si–N distance of 1.853 Å. Note that this is the only compound listed in which SiN_6 octahedra are present in addition to SiN_4 tetrahedra. Two Li compounds also deviate with Li_5SiN_3 having a much larger Si–N distance and $Li_{21}Si_3N_{11}$ having a relatively small distance. Both compounds crystallize in distorted antifluorite structures and both are very Li rich, with the Li and Si atoms present in TN_4 (T = Li, Si) tetrahedra. So, based on their crystal structures both Li_5SiN_3 and $Li_{21}Si_3N_{11}$ are not really nitridosilicates composed of cross-linked tetrahedra such as the other compounds. It has been reported[37] that in $Li_{21}Si_3N_{11}$ the Si is mainly present on the smallest TN_4 site (because Si^{4+} is smaller than Li^+), resulting in a small Si–N bond length. In Li_5SiN_3 on the other hand,
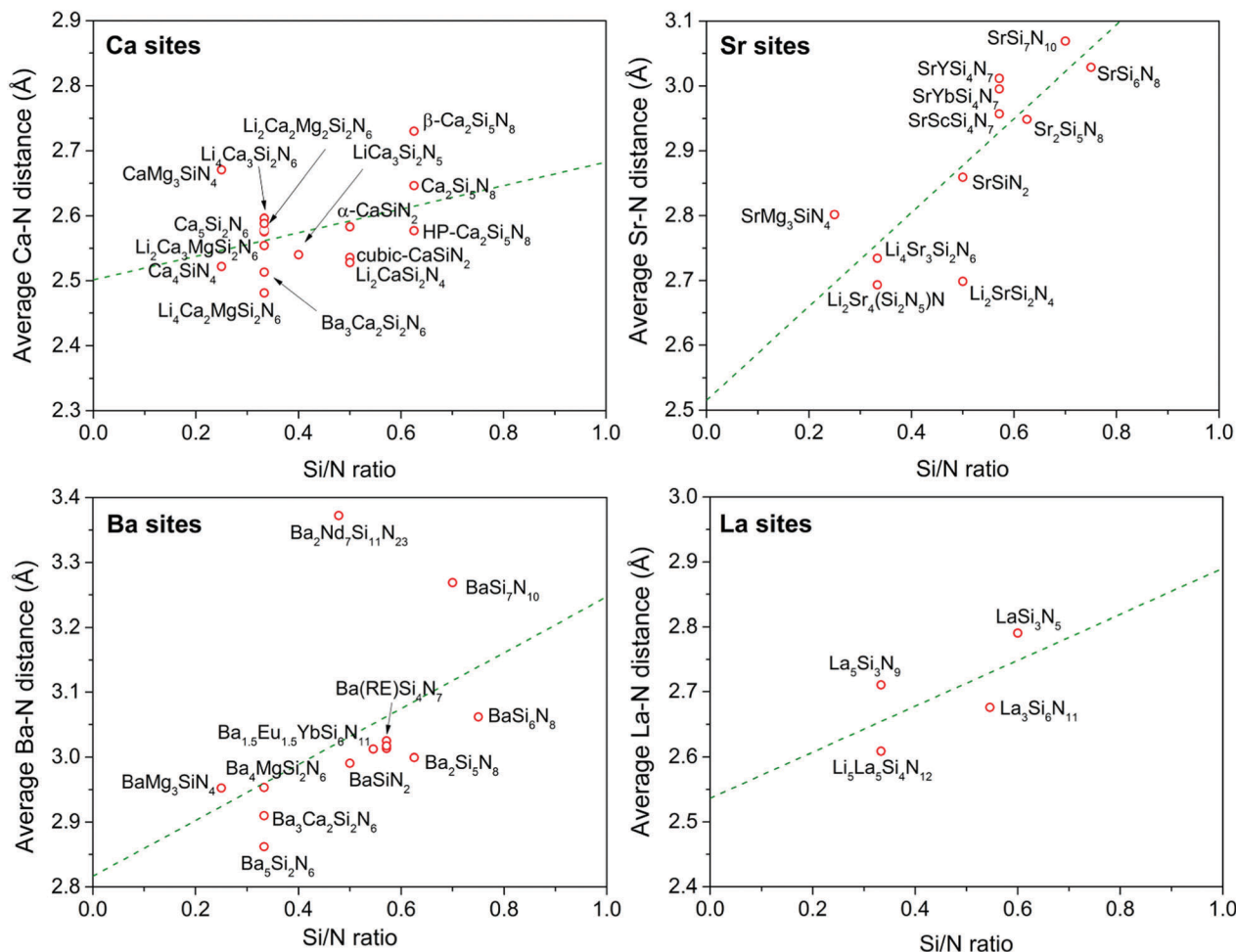
Fig. 4 Average M–N distance (M = Ca, Sr, Ba or La) in the nitridosilicates *versus* the Si/N ratio. The green dashed line represents a trend line obtained by a linear fit through the data points.

Si occupies a mixed Si/Li site making the Si–N distance actually a significantly larger (Si,Li)–N distance. Something similar also happens in $BaMg_3SiN_4$ with mixed Mg/Si sites and thus a large shortest (Mg,Si)–N distance (1.892 Å) since Mg^{2+} is larger than Si^{4+}. The average (Mg,Si)–N distance in $BaMg_3SiN_4$ is also very large (2.030 Å) and falls outside the plotted range of Fig. 5a. In the other (AE)Mg_3SiN_4 compounds (AE = Ca, Sr, Eu) the Mg and Si sites are not mixed and the Si–N bond lengths are as expected for compounds with low Si/N ratio and in the same range as in Ca_4SiN_4. The very small shortest Si–N distance of 1.564 Å reported[54] for $La_5Si_3N_9$ seems to be not reliable, because for $Ce_5Si_3N_9$ and $Pr_5Si_3N_9$, that both crystallize in the same crystal structure as $La_5Si_3N_9$, the reported[54,59] shortest Si–N distances are much larger (1.725 Å for $Ce_5Si_3N_9$ and 1.719 Å for $Pr_5Si_3N_9$) and fall in line with the trend observed in Fig. 5b. Hence that the La^{3+} ion is similar in size as the Ce^{3+} and Pr^{3+} ions. Note that the average Si–N distance in $La_5Si_3N_9$ is not an exception, but in range with the other compounds.

2.3 Bandgap

The bandgaps of the $M_xSi_yN_z$ compounds, listed in Table 2, have been derived from experimental data from literature.

In cases the electrical bandgap E_{VC}, *i.e.* the energy between the top of the valence band and the bottom of the conduction band, has not been reported, E_{VC} is estimated from the exciton creation energy E_{ex}[85,86] or the optical bandgap E_{opt}. For this, absorption or reflectance spectra from undoped compounds and photoluminescence excitation spectra of low concentrated Eu^{2+} or Ce^{3+} doped compounds have been used. For several compounds, the bandgap has been calculated in literature using DFT calculations. These computationally determined bandgaps have not been taken into account as these calculations often tend to underestimate the real value of the bandgap, making comparison with experimentally determined values of other compounds not reliable. More information on the derivation of the bandgap from literature data can be found in the ESI.†

Among the nitridosilicates listed in Table 2, Li_2SiN_2 has the largest bandgap (>6.9 eV) and Li_8SiN_4 has the smallest bandgap (2.7 eV). In general the bandgap increases with increasing Si/N ratio, as shown in Fig. 6. This is in accordance with what was previously predicted by Fang *et al.*[116] using first principle calculations for the barium nitridosilicates: the bandgap increases with increasing degree of cross-linking between SiN_4 tetrahedra in
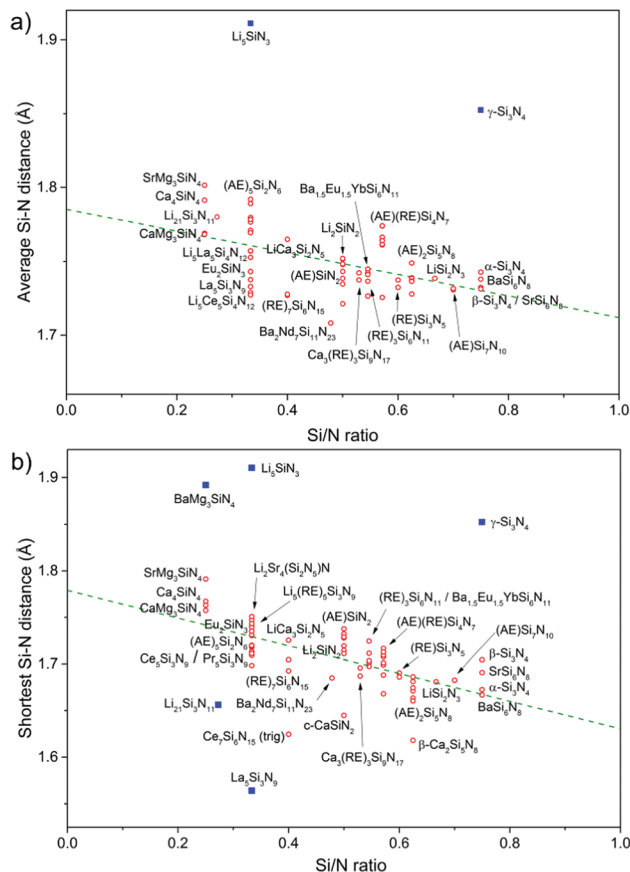
Fig. 5 (a) Average and (b) shortest Si–N distance in the nitridosilicates *versus* the Si/N ratio. The green dashed line represents a trend line obtained by a linear fit through the open red circular data points. The solid blue squared data points are exceptions not included in the fit. The average Si–N distance is defined as the average of all Si–N distances from all SiN₄ tetrahedra; the shortest Si–N distance is defined as the average of all shortest Si–N distances from all SiN₄ tetrahedra.

the order $Ba_5Si_2N_6 < Ba_2Si_5N_8 < BaSi_7N_{10} < \beta\text{-}Si_3N_4$. In the previous section it was explained that with increasing degree of condensation (Si/N ratio) the N atom will get a less negative effective charge. This less negative effective charge will result in a downward shift in energy of the N 2p levels, and because the top of the valence band consists mainly of N 2p levels, this will make the bandgap larger. This is also in line with the calculation by Fang *et al.*,[116] showing a downward shift of the N 2p levels when going from singly coordinated N atoms towards N atoms coordinated by 4 Si atoms.

The increase of the bandgap with increasing degree of condensation is not only caused by a shift of the top of the valence band to lower energy, but should also be partly due to a shift of the bottom of the conduction band to higher energy (with respect to the vacuum level). As was discussed above, the Si–N bond length decreases with increasing Si/N ratio (Fig. 5). The shorter, and therefore stronger bond will give a larger splitting between the bonding orbitals at the top of the valence band (mainly N orbitals) and antibonding orbitals at the bottom of the conduction band (Si orbitals). This will result in a shift of the bottom of the conduction band to higher energy, next to a

Table 2 Bandgap E_{VC} of the nitridosilicates ($M_xSi_yN_z$). The third column specifies the type of experiment from which the bandgap was derived (diffuse reflectance (DR), soft X-rays, optical absorption (ABS), photoluminescence excitation (PLE)) and the corresponding references. See the ESI for more details

Compound	E_{VC} (eV)	Ref.
$\alpha\text{-}Si_3N_4$	5.9	DR[87]
$\gamma\text{-}Si_3N_4$	5.1	X-rays,[88] PLE[89]
Li_8SiN_4	2.7	ABS[26]
Li_5SiN_3	2.8	ABS[90]
$LiSi_2N_3$	6.9	DR,[28] PLE[27]
Li_2SiN_2	>6.9	DR[91]
$MgSiN_2$	5.5	DR,[92,93] X-rays[94]
$\alpha\text{-}CaSiN_2$	5.0	DR,[95,96] PLE[95]
$Ca_{16}Si_{17}N_{34}{}^a$	4.7	ABS,[97] DR[97,98]
$Ca_2Si_5N_8$	5.2	DR,[99] PLE[99,100]
$SrSiN_2$	5.0	ABS,[93] DR,[93,101] PLE[93,101]
$Sr_2Si_5N_8$	5.1	DR,[99,102] PLE[99,100]
$SrSi_6N_8$	3.7	DR,[103] PLE[104]
$BaSiN_2$	4.9	ABS,[93] DR,[93] PLE[93]
$Ba_2Si_5N_8$	5.1	ABS,[105] DR,[99] PLE[99,100]
$BaSi_7N_{10}$	5.8	DR,[106] PLE[107]
$LaSi_3N_5$	5.0	ABS,[108] DR,[109] PLE[109,110]
$CaMg_3SiN_4$	4.1	PLE[68]
$SrMg_3SiN_4$	4.1	DR[68]
$BaMg_3SiN_4$	4.1	DR[69]
$Li_2Ca_2Mg_2Si_2N_6$	4.8	DR[111]
$Li_4Ca_3Si_2N_6$	4.1	ABS,[112] DR,[112] PLE[112]
$CaLaSiN_3$	3.1	DR[113]
$CaYSi_4N_7{}^b$	5.2	DR[114]
$SrYSi_4N_7$	5.2	DR,[76,77,114] PLE[76]
$BaYSi_4N_7$	5.2	DR[77,114,115]

^{a} $Ca_{16}Si_{17}N_{34}$ is also known as cubic-$CaSiN_2$. ^{b} $CaYSi_4N_7$ is actually $Ca_{0.8}Y_{1.2}Si_4N_{6.8}C_{0.2}$.
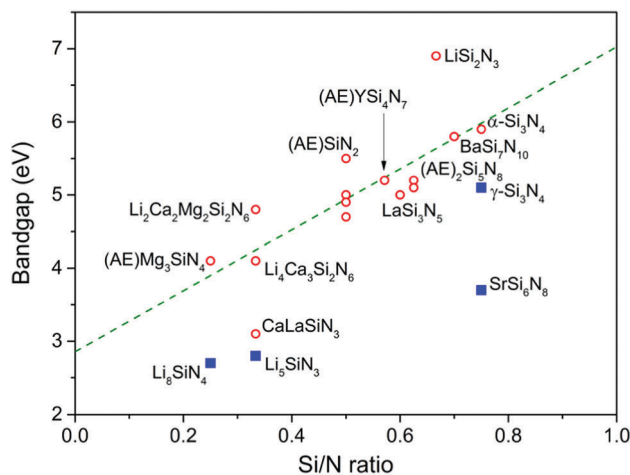
Fig. 6 Bandgap of the nitridosilicates *versus* the Si/N ratio. The green dashed line represents a trend line obtained by a linear fit through the red circular data points. The blue squared data points are exceptions not included for the fit.

shift of the top of the valence band to lower energy. Based on analysis of the thermal quenching behaviour of the Eu^{2+} and Ce^{3+} 5d–4f emission in doped nitridosilicates it can be argued that the bottom of the conduction band should indeed shift upwards in energy with increasing degree of condensation, as will be explained in more detail in our next paper. So the

11510 | *J. Mater. Chem. C*, 2017, 5, 11504–11514

This journal is © The Royal Society of Chemistry 2017

Fig. 7 Schematic diagram, showing the influence of the degree of condensation (Si/N ratio) on the positions of the valence and conduction bands and the size of the bandgap E_g.

increasing bandgap of the nitridosilicates with increasing degree of condensation (increasing Si/N ratio) is the consequence of the combined effect of the downward shift of the valence band and the upward shift of the conduction band as illustrated in Fig. 7. It should be noted here that this model does not take into account that the bottom of the conduction band may not only consist of Si orbitals but may also consist of M orbitals. For example, calculations on the electronic structure of $LaSi_3N_5$ and $La_3Si_6N_{11}$ show that the bottom of the conduction band of these compounds contains La 4f and 5d states.[117] Nevertheless, the calculations still show that $La_3Si_6N_{11}$, which has a lower Si/N ratio, has a smaller bandgap than $LaSi_3N_5$ and a conduction band minimum at lower energy. The smaller bandgap may seem contradictory to the shorter La–N distance in $La_3Si_6N_{11}$, but could be explained by the larger crystal field splitting a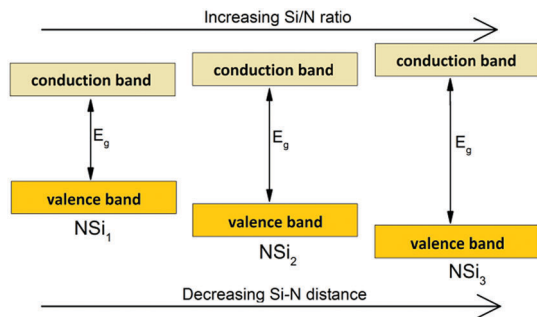nd centroid shift of the 5d levels in $La_3Si_6N_{11}$ as compared to $LaSi_3N_5$, lowering the bottom of the conduction band.

The bandgaps of $SrSi_6N_8$ (about 3.7 eV) and γ-Si_3N_4 (about 5.1 eV) are small considering their high Si/N ratios and deviate from the trend established for the other nitridosilicates. As already mentioned, in γ-Si_3N_4 not all Si atoms are tetrahedrally coordinated by N. The presence of SiN_6 octahedra causes a lowering of the Si 3s states at the bottom of the conduction band.[116] The smaller bandgap is also in line with the larger Si–N bond length in γ-Si_3N_4 as compared to those bonds in α-Si_3N_4 and β-Si_3N_4 (Fig. 5). In $SrSi_6N_8$ as another exception not all Si atoms are tetrahedrally coordinated by N, as part of the Si atoms form Si–Si bonds. The Si–Si bonds create an empty σ^* anti-bonding state forming the bottom of the conduction band, resulting in the smaller bandgap.[118] Therefore it is likely that $BaSi_6N_8$, in which also Si–Si bonds are present, has a relatively small bandgap as well, but to our knowledge its bandgap has not yet been experimentally determined.

For Li_2SiN_2 the exact value of the bandgap is unknown, but it should be larger than 6.9 eV since it has a high reflectivity down to 200 nm radiation.[91] The bandgap is thus very large considering that the Si/N ratio is only 0.5 and in the same range with that of $LiSi_2N_3$, which also has a relatively large bandgap. Such large bandgaps can be attributed to the presence of Li. As Li^+ ions are relatively small, the Li–N bond is short compared to the M–N bond in other nitridosilicates. Instead of considering

the coordination number of N based on the number of Si atoms around it, also the coordinating Li atoms should therefore be taken into account. This increases the $N(Si,Li)_x$ coordination number to about 4 in $LiSi_2N_3$ and even to 6 in Li_2SiN_2, meaning that the effective charge around N becomes more positive, the top of the valence band shifts downwards and the bandgap becomes large. Note that the same reasoning does not apply for Li_5SiN_3 which has a very small bandgap. The Si atoms are here located on the large Li sites, making the (Si,Li)–N bonds much longer (see Fig. 5) and weaker than in $LiSi_2N_3$ and Li_2SiN_2, making it more ionic with a more negative effective charge for N. Something similar may also apply for Li_8SiN_4 as it also has a small bandgap, but the crystal structure of Li_8SiN_4 has not fully been resolved in order to clarify this.

3. Conclusions

With increasing degree of condensation (Si/N ratio) in the nitridosilicates, the coordination number of N by Si increases, the Si–N bond lengths decrease, the M–N bond lengths increase and the bandgap increases as well. This can be understood by considering the changes in effective charge of N and Si–N bond lengths. With a low degree of condensation between the SiN_4 tetrahedra the N atom is under-bonded, giving it an effective negative charge. This effective charge becomes less negative with a higher degree of cross-linking between the SiN_4 tetrahedra, making the M–N bonds weaker and longer. As a result of the less negative effective charge of N, the N 2p levels, and thus the top of the valence band, shift downwards and the bandgap becomes larger. The bandgap is also increased with increasing degree of condensation because the Si–N distance decreases, resulting in a larger splitting between the bonding (N) and antibonding (Si) orbitals. Some compounds, such as γ-Si_3N_4, $SrSi_6N_8$ and several Li containing compounds, show deviations to the general trends, which can be understood based on their differences in structure as compared to the other nitridosilicates, as their framework does not solely consist of cross-linking SiN_4 tetrahedra.

The obtained insights on the relations between bandgap, structure and composition can be used when developing new materials with certain structural or optical properties. For example for the development of novel luminescent materials, for which the positions of the valence and conduction band are of direct influence on the photoluminescence properties.

Although we have focused ourselves in this manuscript on the nitridosilicates, the observed trends are expected to be more general and hold also for other series of compounds whose structure consists of a framework of cross-linked tetrahedra with larger counterions located in the cavities, such as the oxosilicates, oxoaluminates, nitridoaluminates and phosphates. Indeed, a decrease of the Si–O bond length with increasing Si/O ratio has been previously observed for the oxosilicates.[119–121] One can therefore expect that there might also be an increase of the bandgap and increase of the M–O bond length with increasing Si/O ratio. The smaller variation in Si/O ratio among the

This journal is © The Royal Society of Chemistry 2017

J. Mater. Chem. C, 2017, **5**, 11504–11514 | **11511**

oxosilicates *versus* the variation in Si/N ratio among the nitridosilicates may have hampered the establishment of such a relationship so far.

Conflicts of interest

There are no conflicts to declare.

Acknowledgements

Notes and references

1 R. J. Xie and H. T. Hintzen, *J. Am. Ceram. Soc.*, 2013, **96**, 665–687.
2 R. J. Xie and N. Hirosaki, *Sci. Technol. Adv. Mater.*, 2007, **8**, 588–600.
3 R. J. Xie, N. Hirosaki, Y. Q. Li and T. Takeda, *Materials*, 2010, **3**, 3777–3793.
4 R. Mueller-Mach, G. Mueller, M. R. Krames, H. A. Höppe, F. Stadler, W. Schnick, T. Juestel and P. Schmidt, *Phys. Status Solidi A*, 2005, **202**, 1727–1732.
5 R. J. Xie, N. Hirosaki, N. Kimura, K. Sakuma and M. Mitomo, *Appl. Phys. Lett.*, 2007, **90**, 191101.
6 S. E. Brinkley, N. Pfaff, K. A. Denault, Z. J. Zhang, H. T. Hintzen, R. Seshadri, S. Nakamura and S. P. DenBaars, *Appl. Phys. Lett.*, 2011, **99**, 241106.
7 H. T. J. M. Hintzen and M. C. M. Van de Sanden, *U.S. Pat.*, 12/282524, 2007.
8 O. M. ten Kate, M. de Jong, H. T. Hintzen and E. van der Kolk, *J. Appl. Phys.*, 2013, **114**, 084502.
9 K. Van den Eeckhout, P. F. Smet and D. Poelman, *Materials*, 2011, **4**, 980–990.
10 R. Withnall, J. Silver, G. R. Fern, T. G. Ireland, A. L. Lipman and B. Patel, *J. Soc. Inf. Disp.*, 2008, **16**, 359–366.
11 S. Hampshire, *Mater. Sci. Forum*, 2009, **606**, 27–41.
12 M. Zeuner, S. Pagano and W. Schnick, *Angew. Chem., Int. Ed.*, 2011, **50**, 7754–7775.
13 S. Hampshire, H. K. Park, D. P. Thompson and K. H. Jack, *Nature*, 1978, **274**, 880–882.
14 R. J. Xie, N. Hirosaki, M. Mitomo, Y. Yamamoto, T. Suehiro and K. Sakuma, *J. Phys. Chem. B*, 2004, **108**, 12027–12031.
15 J. W. H. van Krevel, J. W. T. van Rutten, H. Mandal, H. T. Hintzen and R. Metselaar, *J. Solid State Chem.*, 2002, **165**, 19–24.
16 K. Uheda, N. Hirosaki, Y. Yamamoto, A. Naito, T. Nakajima and H. Yamamoto, *Electrochem. Solid-State Lett.*, 2006, **9**, H22–H25.
17 R. J. Xie, N. Hirosaki, H. L. Li, Y. Q. Li and M. Mitomo, *J. Electrochem. Soc.*, 2007, **154**, J314–J319.

18 Y. Q. Li, A. C. A. Delsing, G. de With and H. T. Hintzen, *Chem. Mater.*, 2005, **17**, 3242–3248.
19 V. Bachmann, T. Justel, A. Meijerink, C. Ronda and P. J. Schmidt, *J. Lumin.*, 2006, **121**, 441–449.
20 W. Sinclair and A. E. Ringwood, *Nature*, 1978, **272**, 714–715.
21 J. W. H. van Krevel, H. T. Hintzen, R. Metselaar, L. Le Gendre and R. Marchand, *Solid State Sci.*, 2001, **3**, 49–56.
22 Y. Laurent and J. Lang, *C. R. Seances Acad. Sci., Ser. C*, 1966, **262**, 103–106.
23 H. Yamane and H. Morito, *Inorg. Chem.*, 2013, **52**, 5559–5563.
24 M. Zeuner, S. Pagano, P. Matthes, D. Bichler, D. Johrendt, T. Harmening, R. Pöttgen and W. Schnick, *J. Am. Chem. Soc.*, 2009, **131**, 11242–11248.
25 H. Huppertz and W. Schnick, *Chem. – Eur. J.*, 1997, **3**, 249–252.
26 T. Yamashita, S. Kuwano, K. Kuriyama and K. Kushida, *Phys. Status Solidi C*, 2015, **12**, 845–848.
27 J. Y. Ding, Q. S. Wu, Y. Y. Li, Q. Long, C. Wang and Y. H. Wang, *J. Am. Ceram. Soc.*, 2015, **98**, 2523–2527.
28 Y. Q. Li, N. Hirosaki, R. J. Xie, T. Takeka and M. Mitomo, *J. Solid State Chem.*, 2009, **182**, 301–311.
29 P. Dorenbos, *J. Phys.: Condens. Matter*, 2005, **17**, 8103–8111.
30 P. Dorenbos, *J. Phys.: Condens. Matter*, 2003, **15**, 8417–8434.
31 P. Dorenbos, *Chem. Mater.*, 2005, **17**, 6452–6456.
32 K. Liddell, D. P. Thompson and S. J. Teat, *J. Eur. Ceram. Soc.*, 2005, **25**, 49–54.
33 K. Liddell, D. P. Thompson, T. Brauniger and R. K. Harris, *J. Eur. Ceram. Soc.*, 2005, **25**, 37–47.
34 P. Yang, H.-K. Fun, I. A. Rahman and M. I. Saleh, *Ceram. Int.*, 1995, **21**, 137–142.
35 J. Schneider, F. Frey, N. Johnson and K. Laschke, *Z. Kristallogr.*, 1994, **209**, 328–333.
36 J. Z. Jiang, K. Ståhl, R. W. Berg, D. J. Frost, T. J. Zhou and P. X. Shi, *Europhys. Lett.*, 2000, **51**, 62–67.
37 M. Casas-Cabanas, H. Santner and M. R. Palacin, *J. Solid State Chem.*, 2014, **213**, 152–157.
38 R. Juza, H. H. Weber and E. Meyersimon, *Z. Anorg. Allg. Chem.*, 1953, **273**, 48–64.
39 S. Pagano, M. Zeuner, S. Hug and W. Schnick, *Eur. J. Inorg. Chem.*, 2009, 1579–1584.
40 M. Orth and W. Schnick, *Z. Anorg. Allg. Chem.*, 1999, **625**, 1426–1428.
41 R. J. Bruls, H. T. Hintzen, R. Metselaar and C. K. Loong, *J. Phys. Chem. Solids*, 2000, **61**, 1285–1293.
42 P. Bielec and W. Schnick, *Angew. Chem.*, 2017, **129**, 4888–4891.
43 F. Ottinger and R. Nesper, *Z. Anorg. Allg. Chem.*, 2005, **631**, 1597–1602.
44 Z. A. Gál, P. M. Mallinson, H. J. Orchard and S. J. Clarke, *Inorg. Chem.*, 2004, **43**, 3998–4006.
45 S. M. Hick, M. I. Miller, R. B. Kaner and R. G. Blair, *Inorg. Chem.*, 2012, **51**, 12626–12629.
46 T. Schlieper and W. Schnick, *Z. Anorg. Allg. Chem.*, 1995, **621**, 1037–1041.

11512 | *J. Mater. Chem. C*, 2017, **5**, 11504–11514

This journal is © The Royal Society of Chemistry 2017

47 S. R. Römer, C. Braun, O. Oeckler, P. J. Schmidt, P. Kroll and W. Schnick, *Chem. – Eur. J*, 2008, **14**, 7892–7902.

48 T. Schlieper, W. Milius and W. Schnick, *Z. Anorg. Allg. Chem.*, 1995, **621**, 1380–1384.

49 G. Pilet, H. A. Höppe, W. Schnick and S. Esmaeilzadeh, *Solid State Sci.*, 2005, 7, 391–396.

50 F. Stadler, O. Oeckler, J. Senker, H. A. Höppe, P. Kroll and W. Schnick, *Angew. Chem., Int. Ed.*, 2005, **44**, 567–570.

51 H. Yamane and F. J. DiSalvo, *J. Alloys Compd.*, 1996, **240**, 33–36.

52 F. Stadler and W. Schnick, *Z. Anorg. Allg. Chem.*, 2007, **633**, 589–592.

53 H. Huppertz and W. Schnick, *Acta Crystallogr., Sect. C: Cryst. Struct. Commun.*, 1997, **53**, 1751–1753.

54 C. Schmolke, D. Bichler, D. Johrendt and W. Schnick, *Solid State Sci.*, 2009, **11**, 389–394.

55 H. Yamane, T. Nagura and T. Miyazaki, *Acta Crystallogr., Sect. E: Struct. Rep. Online*, 2014, **70**, i23–i24.

56 M. Woike and W. Jeitschko, *Inorg. Chem.*, 1995, **34**, 5105–5108.

57 C. Schmolke, O. Oeckler, D. Bichler, D. Johrendt and W. Schnick, *Chem. – Eur. J.*, 2009, **15**, 9215–9222.

58 T. Schlieper and W. Schnick, *Z. Anorg. Allg. Chem.*, 1995, **621**, 1535–1538.

59 S. Lupart and W. Schnick, *Acta Crystallogr., Sect. E: Struct. Rep. Online*, 2009, **65**, i43.

60 T. Schlieper and W. Schnick, *Z. Kristallogr.*, 1996, **211**, 254.

61 S. Pagano, S. Lupart, S. Schmiechen and W. Schnick, *Z. Anorg. Allg. Chem.*, 2010, **636**, 1907–1909.

62 S. Schmiechen, F. Nietschke and W. Schnick, *Eur. J. Inorg. Chem.*, 2015, 1592–1597, DOI: 10.1002/ejic.201403178.

63 C. Poesl and W. Schnick, *Chem. Mater.*, 2017, **29**, 3778–3784.

64 S. Lupart, S. Pagano, O. Oeckler and W. Schnick, *Eur. J. Inorg. Chem.*, 2011, 2118–2123, DOI: 10.1002/ejic.201100115.

65 S. Lupart and W. Schnick, *Z. Anorg. Allg. Chem.*, 2012, **638**, 2015–2019.

66 M. Zeuner, S. Pagano, S. Hug, P. Pust, S. Schmiechen, C. Scheu and W. Schnick, *Eur. J. Inorg. Chem.*, 2010, 4945–4951.

67 S. Lupart, M. Zeuner, S. Pagano and W. Schnick, *Eur. J. Inorg. Chem.*, 2010, 2636–2641.

68 S. Schmiechen, H. Schneider, P. Wagatha, C. Hecht, P. J. Schmidt and W. Schnick, *Chem. Mater.*, 2014, **26**, 2712–2719.

69 S. Schmiechen, P. Strobel, C. Hecht, T. Reith, M. Siegert, P. J. Schmidt, P. Huppertz, D. Wiechert and W. Schnick, *Chem. Mater.*, 2015, **27**, 1780–1785.

70 H. Yamane and H. Morito, *J. Alloys Compd.*, 2013, **555**, 320–324.

71 O. M. ten Kate, T. Vranken, E. van der Kolk, A. P. J. Jansen and H. T. Hintzen, *J. Solid State Chem.*, 2014, **213**, 126–131.

72 H. Huppertz and W. Schnick, *Angew. Chem., Int. Ed. Engl.*, 1997, **36**, 2651–2652.

73 H. Huppertz, O. Oeckler, A. Lieb, R. Glaum, D. Johrendt, M. Tegel, R. Kaindl and W. Schnick, *Chem. – Eur. J.*, 2012, **18**, 10857–10864.

74 H. Huppertz and W. Schnick, *Z. Anorg. Allg. Chem.*, 1998, **624**, 371–374.

75 D. Porob, N. Karkada, N. P. Kumar and A. Setlur, *ECS Trans.*, 2012, **41**, 27–38.

76 Y. Q. Li, C. M. Fang, G. de With and H. T. Hintzen, *J. Solid State Chem.*, 2004, **177**, 4687–4694.

77 C. M. Fang, Y. Q. Li, H. T. Hintzen and G. de With, *J. Mater. Chem.*, 2003, **13**, 1480–1483.

78 H. Huppertz and W. Schnick, *Z. Anorg. Allg. Chem.*, 1997, **623**, 212–217.

79 R. Marchand, Y. Laurent, J. Lang and M. T. Le Bihan, *Acta Crystallogr., Sect. B: Struct. Sci.*, 1969, **25**, 2157–2160.

80 R. Grün, *Acta Crystallogr., Sect. B: Struct. Sci.*, 1979, **35**, 800–804.

81 Z. Inoue, M. Mitomo and N. Ii, *J. Mater. Sci.*, 1980, **15**, 2915–2920.

82 H. Huppertz and W. Schnick, *Angew. Chem., Int. Ed. Engl.*, 1996, **35**, 1983–1984.

83 A. Zerr, G. Miehe, G. Serghiou, M. Schwarz, E. Kroke, R. Riedel, H. Fueß, P. Kroll and R. Boehler, *Nature*, 1999, **400**, 340–342.

84 W. Schnick and H. Huppertz, *Chem. – Eur. J.*, 1997, **3**, 679–683.

85 P. Dorenbos, *J. Lumin.*, 2005, **111**, 89–104.

86 P. Dorenbos, *Opt. Mater.*, 2017, **69**, 8–22.

87 Y. Q. Li, N. Hirosaki, R. J. Xie, T. Takeda and M. Mitomo, *J. Lumin.*, 2010, **130**, 1147–1153.

88 T. Boyko, A. Hunt, A. Zerr and A. Moewes, *Phys. Rev. Lett.*, 2013, **111**, 097402.

89 L. Museur, A. Zerr and A. Kanaev, *Sci. Rep.*, 2016, **6**, 18523.

90 Y. Takeuchi, T. Yamashita, K. Kuriyama and K. Kushida, *J. Solid State Electrochem.*, 2016, **20**, 1885–1888.

91 J. Y. Ding, Y. Y. Li, Q. S. Wu, Q. Long, C. Wang and Y. H. Wang, *J. Mater. Chem. C*, 2015, **3**, 8542–8549.

92 G. P. Dubrovskii, A. M. Zykov and B. V. Chernovets, *Inorg. Mater.*, 1981, **17**, 1059–1063.

93 C. J. Duan, X. J. Wang, W. M. Otten, A. C. A. Delsing, J. T. Zhao and H. T. Hintzen, *Chem. Mater.*, 2008, **20**, 1597–1605.

94 T. de Boer, T. D. Boyko, C. Braun, W. Schnick and A. Moewes, *Phys. Status Solidi RRL*, 2015, **9**, 250–254.

95 Y. Q. Li, N. Hirosaki, R. J. Xie, T. Takada, Y. Yamamoto, M. Mitomo and K. Shioi, *Int. J. Appl. Ceram. Technol.*, 2010, 7, 787–802.

96 X. M. Wang, X. Zhang, S. Ye and X. P. Jing, *Dalton Trans.*, 2013, **42**, 5167–5173.

97 H. Chen, J. Ding, X. Ding, X. Wang, Y. Cao, Z. Zhao and Y. Wang, *Inorg. Chem.*, 2017, **56**, 10904–10913.

98 W. A. Groen, M. J. Kraan and G. Dewith, *J. Mater. Sci.*, 1994, **29**, 3161–3166.

99 Y. Q. Li, J. E. J. van Steen, J. W. H. van Krevel, G. Botty, A. C. A. Delsing, F. J. DiSalvo, G. de With and H. T. Hintzen, *J. Alloys Compd.*, 2006, **417**, 273–279.

100 Y. Q. Li, G. de With and H. T. Hintzen, *J. Lumin.*, 2006, **116**, 107–116.

101 L. Chen, R. H. Liu, W. D. Zhuang, Y. H. Liu, Y. S. Hu, X. L. Ma and B. Hu, *J. Rare Earths*, 2016, **34**, 30–35.

This journal is © The Royal Society of Chemistry 2017

J. Mater. Chem. C, 2017, **5**, 11504–11514 | **11513**

102 X. Q. Piao, T. Horikawa, H. Hanzawa and K. Machida, *Appl. Phys. Lett.*, 2006, **88**, 161908.

103 K. Shioi, N. Hirosaki, R. J. Xie, T. Takeda and Y. Q. Li, *J. Mater. Sci.*, 2008, **43**, 5659–5661.

104 C.-W. Yeh, Y.-P. Liu, Z. R. Xiao, Y.-K. Wang, S.-F. Hu and R.-S. Liu, *J. Mater. Chem.*, 2012, **22**, 5828–5834.

105 X. Piao, K. I. Machida, T. Horikawa and H. Hanzawa, *Appl. Phys. Lett.*, 2007, **91**, 041908.

106 Y. Q. Li, A. C. A. Delsing, R. Metslaar, G. de With and H. T. Hintzen, *J. Alloys Compd.*, 2009, **487**, 28–33.

107 J. L. Qin, H. R. Zhang, B. F. Lei, H. W. Dong, Y. L. Liu, J. X. Meng, M. T. Zheng and Y. Xiao, *J. Lumin.*, 2014, **152**, 230–233.

108 O. M. ten Kate, H. T. Hintzen, P. Dorenbos and E. van der Kolk, *J. Mater. Chem.*, 2011, **21**, 18289–18294.

109 T. Suehiro, N. Hirosaki, R. J. Xie and T. Sato, *Appl. Phys. Lett.*, 2009, **95**, 051903.

110 Y. Zhou, Y. I. Yoshizawa, K. Hirao, Z. Lenčéš and P. Šajgalík, *J. Eur. Ceram. Soc.*, 2011, **31**, 151–157.

111 P. Strobel, V. Weiler, C. Hecht, P. J. Schmidt and W. Schnick, *Chem. Mater.*, 2017, **29**, 1377–1383.

112 Q. Wu, J. Ding, Y. Li, X. Wang and Y. Wang, *J. Lumin.*, 2017, **186**, 144–151.

113 O. M. ten Kate, H. T. Hintzen and E. van der Kolk, *J. Phys.: Condens. Matter*, 2014, **26**, 385502.

114 T. Kurushima, G. Gundiah, Y. Shimomura, M. Mikami, N. Kijima and A. K. Cheetham, *J. Electrochem. Soc.*, 2010, **157**, J64–J68.

115 Y. Q. Li, G. de With and H. T. Hintzen, *J. Alloys Compd.*, 2004, **385**, 1–11.

116 C. M. Fang, H. T. Hintzen and G. De With, *Recent Res. Dev. Mater. Sci.*, 2003, **4**, 283–291.

117 Y. Jia, A. Miglio, S. Poncé, X. Gonze and M. Mikami, *Phys. Rev. B*, 2016, **93**, 155111.

118 Z. Huang, F. Chen, J. Zhang, Q. Shen and L. Zhang, *RSC Adv.*, 2017, **7**, 8779–8785.

119 W. H. Baur, *Acta Crystallogr., Sect. B: Struct. Sci.*, 1978, **34**, 1751–1756.

120 G. E. Brown and G. V. Gibbs, *Am. Mineral.*, 1969, **54**, 1528–1539.

121 J. V. Smith and S. W. Bailey, *Acta Crystallogr.*, 1963, **16**, 801–811.